Chemical Science

ROYAL SOCIETY OF CHEMISTRY

EDGE ARTICLE

View Article Online
View Journal | View Issue

Cite this: *Chem. Sci.*, 2021, **12**, 9069

All publication charges for this article have been paid for by the Royal Society of Chemistry

Low power threshold photochemical upconversion using a zirconium(IV) LMCT photosensitizer†

Mo Yang, [a] Sara Sheykhi, [a] Yu Zhang, [b] Carsten Milsmann [b] and Felix N. Castellano *[a]

The current investigation demonstrates highly efficient photochemical upconversion (UC) where a long-lived Zr(IV) ligand-to-metal charge transfer (LMCT) complex serves as a triplet photosensitizer in concert with well-established 9,10-diphenylanthracene (DPA) along with newly conceived DPA–carbazole based acceptors/annihilators in THF solutions. The initial dynamic triplet–triplet energy transfer (TTET) processes ($\Delta G \sim -0.19$ eV) featured very large Stern–Volmer quenching constants (K_{SV}) approaching or achieving 10^5 M^{-1} with bimolecular rate constants between 2 and 3 $\times$ 10^8 M^{-1} s^{-1} as ascertained using static and transient spectroscopic techniques. Both the TTET and subsequent triplet–triplet annihilation (TTA) processes were verified and throughly investigated using transient absorption spectroscopy. The Stern–Volmer metrics support 95% quenching of the Zr(IV) photosensitizer using modest concentrations (0.25 mM) of the various acceptor/annihilators, where no aggregation took place between any of the chromophores in THF. Each of the upconverting formulations operated with continuous-wave linear incident power dependence (λ_{ex} = 514.5 nm) down to ultralow excitation power densities under optimized experimental conditions. Impressive record-setting η_{UC} values ranging from 31.7% to 42.7% were achieved under excitation conditions (13 mW cm^{-2}) below that of solar flux integrated across the Zr(IV) photosensitizer's absorption band (26.7 mW cm^{-2}). This study illustrates the importance of supporting the continued development and discovery of molecular-based triplet photosensitizers based on earth-abundant metals.

Received 23rd March 2021
Accepted 1st June 2021

DOI: 10.1039/d1sc01662h

rsc.li/chemical-science

Introduction

Triplet–triplet annihilation-based photon upconversion (TTA-UC) represents a strategy enabling low-power anti-Stokes wavelength-shifting as well as energetic photochemical activation.[1–3] TTA-UC is initialized through selective long-wavelength excitation of a strongly-absorbing triplet photosensitizer. The electronically excited triplet photosensitizer then engages in collisional triplet–triplet energy transfer (TTET) with an energetically-appropriate acceptor chromophore. Triplet–triplet annihilation (TTA) between two excited triplet acceptors ultimately forms one singlet acceptor excited state, thereby emanating fluorescence at higher energy with respect to the excitation.[4–6] More generally, the excited state ultimately produced can be leveraged for myriad applications, including photovoltaics,[7–10] photocatalysis,[11–14] biological imaging[15,16] and photodynamic therapy.[17,18] However, realizing high normalized upconversion efficiency values (η_{UC}), where $\eta_{UC} \geq 20\%$ at or below solar irradiance, remains a significant scientific challenge.[19]

Synthetic advances enabling control of the photophysical properties of transition metal complexes and materials are revolutionizing triplet sensitization.[20–29] Numerous molecular triplet sensitizers featuring long-lived excited states contain

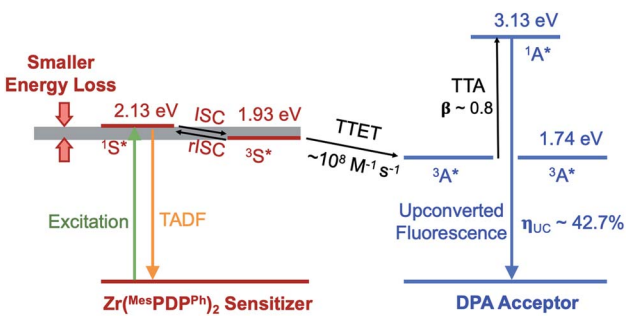

Fig. 1 Energy-level diagram representing the photophysical and photochemical processes of the Zr(^{Mes}PDP^{Ph})$_2$/DPA donor–acceptor system. S = sensitizer and A = acceptor/annihilator.

[a]Department of Chemistry, North Carolina State University, Raleigh, North Carolina 27695-8204, USA. E-mail: fncastel@ncsu.edu

[b]C. Eugene Bennett Department of Chemistry, West Virginia University, Morgantown, West Virginia 26506, USA. E-mail: camilsmann@mail.wvu.edu

† Electronic supplementary information (ESI) available: Synthesis of CzPA, F–CzPA and CN–CzPA, ^{1}H NMR spectra, DOSY spectra, ROESY spectra, upconverted photoluminescence spectra, transient absorption spectra and kinetic analysis, double logarithmic plots, Stern–Volmer analysis and calculated energies. See DOI: 10.1039/d1sc01662h

rare-earth and precious second- or third-row transition metals, including Ru(II),[30–33] Ir(III),[34–37] Re(I),[38,39] Pt(II) or Pd(II).[5,40–42] Replacing precious metals with more earth-abundant transition metals reveals additional non-radiative decay pathways that markedly attenuate excited state lifetimes.[43,44] However, significant progress has been made using Cu(I) metal-to-ligand charge-transfer (MLCT) complexes featuring d^{10} configurations that eliminate ligand-field deactivation processes.[21,45–48] Another molecular design that effectively deletes ligand-field states is based on d^0 ligand-to-metal charge transfer (LMCT) excited states. Newly conceived molecules constructed from Zr(IV) platforms are extremely attractive in this regard,[49–52] featuring high quantum yield thermally-activated delayed fluorescence (TADF), Fig. 1. Metal-containing TADF photosensitizers are valuable for photochemical conversion reactions as the closely-spaced singlet–triplet gap conserves energy in intersystem crossing with respect to more traditional triplet photosensitizers. From recent investigations, a strongly-absorbing, air- and moisture-stable Zr(IV) LMCT complex, $Zr(^{Mes}PDP^{Ph})_2$ ($^{Mes}PDP^{Ph}$ = 2,6-bis(5-(2,4,6-trimethylphenyl)-3-phenyl-1*H*-pyrrol-2-yl)pyridine) (Fig. 2A) has emerged, featuring a long-lived triplet excited state of 350 μs at RT.[51] Although such molecules have been used in photoredox catalysis,[49–51] to the best of our knowledge, there are no examples of LMCT excited states being harnessed in upconversion schemes to date.

Here, we report unprecedented low-power threshold photochemical upconversion systems using the LMCT photosensitizer $Zr(^{Mes}PDP^{Ph})_2$ in combination with 9,10-diphenylanthracene (DPA) and newly conceived carbazole-based DPA derivatives (CzPA) as acceptors/annihilators.[53–56] The relative singlet and triplet energy levels of these chromophores are presented in Fig. 1 along with their relevant TADF (ISC/rISC) and TTET processes. The $Zr(^{Mes}PDP^{Ph})_2$/DPA combination achieved record (42.7 ± 0.3)% quantum efficiency (normalized) under low fluence (13 mW cm^{-2}) continuous-wave excitation using low chromophore concentrations. The remaining CzPA chromophores realized efficiencies ranging between 31.7–42.7% in conjunction with the Zr(IV) sensitizer using similar photon flux and experimental conditions, representing next generation acceptors/annihilators poised for high yield annihilation photochemistry. The realization of high quantum yield upconversion below solar flux using modest chromophore concentrations will likely inspire researchers to broadly employ this tool as a standard photochemical activation strategy for numerous applications.

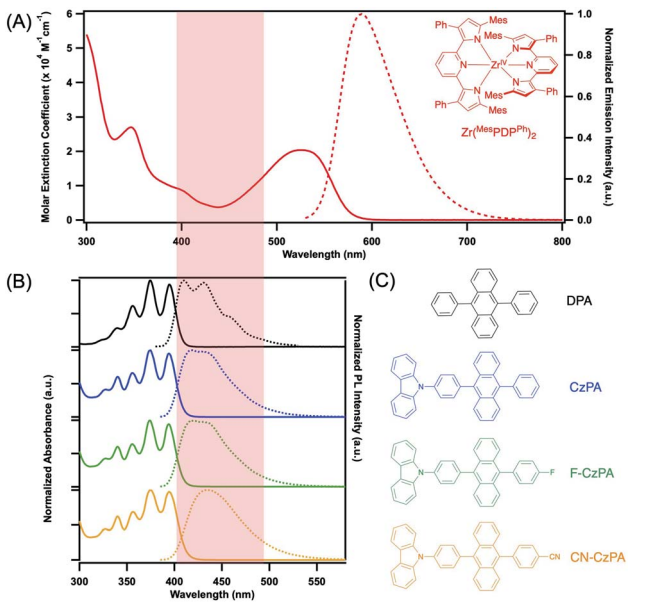

Fig. 2 (A) Electronic absorption (solid line) and photoluminescence (dashed line) spectra of $Zr(^{Mes}PDP^{Ph})_2$ in THF. (B) Normalized absorption (solid lines) and photoluminescence (dashed lines) spectra of DPA (black), CzPA (blue), F–CzPA (green) and CN–CzPA (orange). The red shaded area shows a small spectral overlap between photoluminescence of acceptors and absorbance of $Zr(^{Mes}PDP^{Ph})_2$, indicating minimal reabsorption of upconverted fluorescence by the sensitizer. (C) Chemical structures of DPA (black), CzPA (blue), F–CzPA (green) and CN–CzPA (orange).

Experimental

General

$Zr(^{Mes}PDP^{Ph})_2$ was synthesized and purified as previously reported and its relevant NMR spectra are provided as ESI.†[51] CzPA was prepared according to the established literature method.[56] F–CzPA and CN–CzPA were synthesized by modifying previously reported procedures[57] and purified by vacuum sublimation, please see the ESI† for details. Details regarding all solution-based structural characterization using ^1H and ^{13}C NMR spectroscopy are described in the ESI.† 9,10-Diphenylanthracene (DPA) was purchased from Alfa Aesar and used without further purification. Spectroscopic samples were prepared in an inert atmosphere (N_2-filled) glovebox (MBraun) using spectrophotometric grade tetrahydrofuran (THF), which was previously deoxygenated and dried using a glass contour solvent purification system (MBraun). Spectroscopic solutions were measured in air-free 1 cm^2 quartz optical cells. Static absorption spectra were acquired using a Cary 60 spectrophotometer. Steady-state photoluminescence spectra were collected using a FS-920 spectrofluorometer (Edinburgh Instruments) equipped with a 450 W Xe arc lamp/monochromator combination as the excitation source and a Peltier cooled, red-sensitive photomultiplier tube detector (R2658P Hamamatsu). Photoluminescence spectra were corrected for emission detector response using an NBS calibrated light source (NIST). Absolute fluorescence quantum yields were measured using a FS-5 spectrofluorometer (Edinburgh Instruments) equipped with an integrating sphere module. This module comprises of a hollow sphere with 150 mm internal diameter with the inner surface machined from a PTFE-based material for optimum reflectance (Edinburgh Instruments).

Absolute fluorescence quantum yields

Optically dilute solutions (OD = 0.1–0.2) of the CzPA series acceptor/annihilator chromophores were used to record their fluorescence spectra in aerated THF using 370 nm excitation.

Absolute fluorescence quantum yields were measured using an integrating sphere in the ambient. This absolute method requires two measurements: the number of absorbed photons and the number of the emitted photons. The number of absorbed photons in each sample was determined by the reduction of the light scattering compared to a solvent blank measurement. The quantum yield calculation was performed using the wizard within the Fluoracle software (version 2.6.1) module (Edinburgh Instruments).

Incident light-power dependence in photochemical upconversion

The concentration of the photosensitizer $Zr(^{Mes}PDP^{Ph})_2$ was chosen to give an absorbance of 0.2 at the excitation wavelength of 514.5 nm, and the concentrations of acceptors/annihilators were selected to quench > 95% of the sensitizer photoluminescence, based on the respective K_{SV} values obtained from Stern–Volmer analysis. The 514.5 nm line of an Ar^+/Kr^+ ion laser (Innova 70-C from Coherent), focused to a 1.0 mm spot, was used as the excitation source. The excitation power density was measured using a Nova II/PD 300-UV energy meter (Ophir). An appropriate long-pass filter (500 nm) and 514.5 nm bandpass filter was used to filter the excitation beam to prevent direct excitation of the acceptor from laser plasma lines. A 310–550 nm bandpass filter was positioned between the sample and the detector to enable anti-Stokes photoluminescence detection. No photoluminescence was observed when neat solutions of the acceptors/annihilators were excited at 514.5 nm under all experimental conditions. The excitation laser power densities were adjusted using a variety of neutral density filters, positioned between the incident light and the sample. The integrated photoluminescence intensities generated were plotted against the measured excitation power densities.

Photochemical upconversion quantum efficiencies

Sample conditions here echo those used in the incident light-power dependence experiments described above. Normalized upconversion quantum efficiencies (η_{UC})[6] were calculated relative to the $[Ru(bpy)_3]Cl_2$ standard in aerated water ($\Phi_{std} = 0.04 \pm 0.002$)[58] according to the following equation:

$$\eta_{UC} = 2\Phi_{std}\left(\frac{A_{std}}{A_{UC}}\right)\left(\frac{I_{UC}}{I_{std}}\right)\left(\frac{n_{THF}}{n_{std}}\right)^2 \quad (1)$$

where η_{UC}, A_{UC}, I_{UC} and n_{THF} represent the upconversion quantum efficiency, sample absorbance at 514 nm, integrated photoluminescence intensity and refractive index of the solvent of the upconversion sample, respectively. The corresponding terms for the subscript "std" are for the reference quantum counter at the corresponding excitation wavelength. The refractive index of the solvents used were $n_{water} = 1.333$ and $n_{THF} = 1.407$ at 20 °C. The factor of 2 is included in eqn (1) because upconversion requires the absorption of two incident photons to produce one highly energized photon, enabling clear comparisons to most of the available literature data, namely, normalized upconversion efficiency (η_{UC}) values.[6]

Dynamic Stern–Volmer analyses

The Stern–Volmer constants (K_{SV}) and the bimolecular quenching constants (k_q) were obtained according to the dynamic Stern–Volmer relation (eqn (2)):

$$\frac{I_0}{I} = \frac{\tau_0}{\tau} = 1 + K_{SV}[Q] \quad (2)$$

where I_0 and I are the Zr(IV) sensitizer photoluminescence intensities in the absence or presence of the quencher, respectively, and τ_0 and τ are the sensitizer lifetimes in the absence or presence of the quencher, respectively. K_{SV} is the Stern–Volmer constant, $K_{SV} = k_q\tau_0$, and [Q] is the molar concentration of triplet quencher. The lifetimes of the Zr(IV) photosensitizer determined from photoluminescence intensity decays were adequately modelled using a single exponential function for all quencher concentrations utilized. The slopes of the Stern–Volmer plots were linear over the entire range of measured quencher concentrations in all instances.

Nanosecond transient absorption spectroscopy

Nanosecond transient absorption difference spectra and kinetics were measured using an Edinburgh Instruments LP-920 laser flash photolysis system equipped with a pulsed 450 W Xe arc lamp and an iStar iCCD Camera (Andor) serving as the detector at the exit port of a spectrograph. The laser excitation pump source was a Vibrant LD 355 II ND: YAG/OPO system from OPOTEK. The differential transient absorption spectra were recorded in deaerated THF following pulsed nanosecond laser excitation ($\lambda_{ex} = 514$ nm, 2 mJ per pulse, 5–7 ns fwhm). The optical density in each sample was maintained between 0.3–0.5 OD at the excitation wavelength. Single wavelength kinetic traces were measured by using a monochromator and PMT detector (R-928 Hamamatsu), with data acquisition controlled by the Edinburgh Instruments LP 900 software. The single wavelength absorbance transients of the Zr(IV) photosensitizer were single exponential in all instances. The recorded single wavelength kinetic decays of each triplet acceptor/annihilator following triplet sensitization were adequately fit to a model equation following parallel first-and second-order kinetics[22,59] in Igor Pro 7.08 software. Please see the model equations (eqn (S1)–(S3)†) for more details.

Results and discussion

Molecular photophysics

The electronic and photoluminescence spectra of $Zr(^{Mes}PDP^{Ph})_2$ measured in THF (Fig. 2A) are consistent with the previous study.[51] $Zr(^{Mes}PDP^{Ph})_2$ exhibits an intense absorption band centred at 525 nm ($\varepsilon_{525} = 21\,570\ M^{-1}\ cm^{-1}$), assigned to having mixed singlet intra-ligand (^{1}IL) and ^{1}LMCT character.[51] The static photoluminescence spectrum of the Zr(IV) complex displays a broad and featureless emission band with a maximum at 581 nm, mirroring the shape of the lowest-energy absorption band. The CzPA series of acceptors/annihilators possess similar spectroscopic signatures to the benchmark DPA chromophore, presented in Fig. 2B. The absorption bands

in the range of 340–410 nm are assigned to $\pi \rightarrow \pi^*$ transitions of the DPA unit.[56] Absolute fluorescence quantum yields measured in THF solutions yielded Φ_F = 81.6%, 82.5% and 74.7% for CzPA, F–CzPA and CN–CzPA, respectively. As the electron-withdrawing ability increased from the –F to the –CN substituents, the fluorescence spectra progressively red-shifted becoming more featureless. This progression is consistent with the manifestation of smaller HOMO–LUMO gaps featuring increasing degrees of charge-transfer character. This is in excellent agreement with the electronic structure calculations presented in Table S1 and Fig. S8.† Moreover, the minimal spectral overlap between the fluorescence of these acceptors/annihilators and the electronic absorption spectrum of the Zr(IV) sensitizer minimizes reabsorption of the upconverted fluorescence by the sensitizer, thereby reducing potential losses in upconversion efficiency, η_{UC}. We note that akin to DPA, the ^{1}H and ^{13}C NMR spectra of each acceptor show no evidence whatsoever of any aggregation or self-assembly in the ground state at millimolar concentrations, Fig. S2–S7.† These newly conceived molecules therefore seem particularly suitable for pairing with Zr(IV) sensitizers in photochemical upconversion schemes.

Triplet energy transfer

In order to investigate the relevant bimolecular TTET processes and ultimately optimize the quenching conditions for UC, both lifetime and photoluminescence intensity decay of the Zr(IV) sensitizer (see Fig. S11–S14† for details) were examined by Stern–Volmer analysis, eqn (2). We note that there was no evidence of any self-quenching from the Zr(IV) photosensitizer and the lifetime remained constant as a function all concentrations utilized, τ_0 = (358 ± 9) μs. Stern–Volmer quenching constants (K_{SV}) and bimolecular energy transfer quenching rate constants (k_q) for each Zr(IV)/acceptor pair are collected in Table 1. The K_{SV} values obtained from lifetime and photoluminescence intensity measurements were consistent for each Zr(IV)/acceptor pair, revealing exclusive dynamic quenching behaviour for each triplet–triplet energy transfer process. The Stern–Volmer analysis revealed rather strong quenching for these exothermic triplet energy transfers, with K_{SV} values ranging from 7.78 × 10^4 to 1.00 × 10^5 M^{-1} and k_q values ranging from 2.10 × 10^8 to 2.71 × 10^8 M^{-1} s^{-1}. The large K_{SV} values are consistent with the long excited state lifetime of sensitizer being used (~358 μs),[59] enabling 95% quenching of the sensitizer using modest concentrations of donor (10.1 μM) and acceptor (0.25 mM) in each instance. The linearity exhibited by the collective Stern–Volmer plots along with TTET quenching below the diffusion limit suggest that no aggregation is occurring between the Zr(IV) photosensitizers and the acceptors/annihilators. This indirect evidence was confirmed using diffusion ordered spectroscopy (DOSY) and rotating frame Overhauser spectroscopy (ROESY) ^{1}H NMR. These 2D-NMR techniques enabled us to monitor any possible aggregation in upconversion mixtures by directly correlating diffusion

Table 1 Performance metrics of Zr(IV)-sensitized photochemical upconversion as a function of acceptor

Acceptor	Φ_F[a] (%)	η_{UC}[b] (%)	K_{SV}[c] (×10^4 M^{-1})	k_q[c] (×10^8 M^{-1} s^{-1})	E_{abs}[d] (eV)	E_{em}[e] (eV)	ΔE[f] (eV)
DPA	94.0 (ref. 82)	42.7 ± 0.3	8.25 ± 0.65	2.48 ± 0.19	2.36	3.02	0.66
CzPA	81.6	37.4 ± 0.2	10.0 ± 0.99	2.71 ± 0.27	2.36	2.95	0.59
F–CzPA	82.5	37.8 ± 0.4	7.78 ± 1.02	2.10 ± 0.28	2.36	2.95	0.59
CN–CzPA	74.7	31.7 ± 0.2	9.25 ± 0.85	2.56 ± 0.24	2.36	2.86	0.50

[a] Fluorescence quantum yield of acceptors/annihilators. [b] Upconversion quantum efficiency limit is 1. Reported values are the average upconversion quantum efficiencies in the plateau region. [c] Reported values are the average of the two values extracted from Stern–Volmer analysis of photoluminescence intensity data and lifetime data. [d] The peak maxima of the lowest energy absorption band of Zr(^{Mes}PDP^{Ph})$_2$. [e] The peak maxima of the highest energy band in the corrected upconverted fluorescence spectra. [f] Apparent anti-Stokes shift,[6] $\Delta E = E_{em} - E_{abs}$.

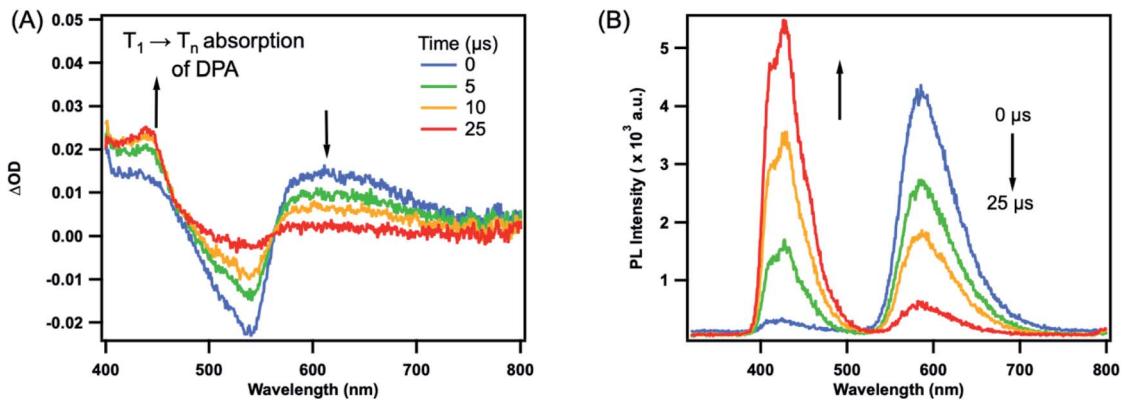

Fig. 3 Transient absorption difference spectra (A), and time-resolved photoluminescence spectra (B) of Zr(^{Mes}PDP^{Ph})$_2$ ($OD_{514\ nm}$ = 0.4) and 0.25 mM DPA in deaerated THF at several delay times following 514 nm pulsed laser excitation (~2 mJ per pulse) with delay times indicated.

coefficients and chemical shifts. Identical diffusion coefficients, $D \sim 3.3 \times 10^{-5}$ cm^2 s^{-1}, were determined for the independent CzPA chromophore and the Zr(^{Mes}PDP^{Ph})$_2$/CzPA mixture in THF using the DOSY spectra. These experiments support the conclusion that no aggregation or self-assembly of the chromophores takes place in solution (Fig. S15†). Additionally, the ROESY spectrum displayed in Fig. S16† shows no evidence of intermolecular interactions between Zr(^{Mes}PDP^{Ph})$_2$ and CzPA, consistent with the collective static and dynamic photophysical data.

The TTET processes were further investigated using nanosecond transient absorption spectroscopy where the Zr(IV) photosensitizer was selectively excited at 514 nm. Fig. 3 presents the spectroscopic investigation of triplet energy transfer from Zr(^{Mes}PDP^{Ph})$_2$ sensitizer to DPA, serving as a representative example for the entire series. The remaining TTET processes involving the CzPA-based acceptors/annihilators are presented in Fig. S17–S19.† The nanosecond transient absorption spectra, Fig. 3A, showed a ^{3}DPA* characteristic $T_1 \rightarrow T_n$ absorption band between 420–450 nm that formed during the initial timescale of 0–25 μs, and then decayed upon repopulating the ground state on longer time scales. Time-resolved photoluminescence spectra, Fig. 3B, indicated the growth of DPA fluorescence synchronous with the decay of photoluminescence of the Zr(IV) sensitizer, consistent with TTA generating singlet fluorescence in DPA. The absence of DPA radical cation or anion bands in the region of 550–750 nm (ref. 60) eliminates the possibility of electron transfer reactions occurring in parallel. These collective experimental observations are consistent with the photoluminescence quenching being a result of TTET from Zr(^{Mes}PDP^{Ph})$_2$ to the various acceptors/annihilators.

Bimolecular TTA rate constants (k_{TTA}) for these Zr(^{Mes}PDP^{Ph})$_2$/acceptor UC systems were determined from transient absorption decay kinetics of the acceptors/annihilators (^{3}A*) measured as a function of laser pulse energy at 514 nm. Kinetic analysis of all the UC pairs used our previously reported approach[22,59] (see eqn (S1)–(S4)† for details) where the sensitized triplet acceptors follow parallel first-(intrinsic triplet decay, k_T) and second-order (TTA process, k_{TTA}) kinetics. In the case of DPA presented in Fig. S20,† the transient kinetics at 450 nm (characteristic of the DPA* $T_1 \rightarrow T_n$ absorption band) was fit to eqn (S3).† The near diffusion-limited TTA rate constants, $k_{TTA} \sim 10^9$ M^{-1} s^{-1} were one order-of-magnitude greater than the precursory bimolecular TTET process determined by Stern–Volmer analysis. With increasing laser pulse energy, the initial concentration of acceptor/annihilator triplets, [^{3}A*], the TTA rate, α ($\alpha = k_{TTA} \times [^3A^*]$), and the initial fractions of ^{3}A* decay occurring through second-order TTA, β, progressively increased or fluctuated around the maxima while the first-order decay rate, k_T, remained constant at $\sim 10^3$ s^{-1} (Tables S2–S5†). The kinetic parameters, k_T and k_{TTA}, are consistent with values previously reported for other UC systems incorporating DPA acceptors.[59,61] Additionally, the kinetic analysis for each Zr(^{Mes}PDP^{Ph})$_2$/acceptor UC pair resulted in large β values, ranging between 0.61 to 0.95, illustrating that the majority of sensitized ^{3}A* engages in high efficiency TTA in every composition investigated.

Continuous-wave photochemical upconversion

Selective excitation of the Zr(^{Mes}PDP^{Ph})$_2$ sensitizer at 514.5 nm in the absence of the acceptors/annihilators only resulted in the observations of normal Stokes-shifted photoluminescence characteristic of the Zr(IV) species. The anti-Stokes singlet fluorescence characteristic of each acceptor/annihilator was readily observed using either coherent or non-coherent excitation source in the presence of the Zr(IV) photosensitizer under 514.5 nm excitation, Fig. 4 and S9.† The blue upconverted light was readily discernible with the naked eye in each composition. The incident light power dependence is also presented for each optimized donor–acceptor pair in Fig. 4. Surprisingly, over the entire range of incident fluences utilized, only linear power dependence was observed, even down to low microwatt power levels. These data are consistent with TTA occurring in the strong annihilation regime where the second-order TTA processes outcompete first-order decay of ^{3}A*.[62,63] In order to verify these results, the Zr(^{Mes}PDP^{Ph})$_2$/DPA UC system was prepared using non-optimized TTET quenching conditions to lower both sensitizer concentrations and the TTET reaction efficiency. Under non-optimized quenching conditions, the characteristic transition from quadratic to linear incident light power dependence was readily identified (Fig. S10†), confirming that the anti-Stokes fluorescence indeed results from TTA and not from inadvertent excitation of the acceptor/annihilator molecules. Since we were unable to directly observe the power density threshold (I_{th}) under experimentally optimized conditions, we estimated the theoretical I_{th} value based on the established model equation (eqn (S5)†).[64,65] By measuring experimental I_{th} values using two distinct non-optimized UC conditions (Fig. S10†), we estimated the I_{th} value under optimized conditions, see ESI† for complete details. The calculated I_{th} value for the current UC system was estimated as 0.115 ± 0.038 mW cm^{-2}, in line with our experimental results.

All of the Zr(^{Mes}PDP^{Ph})$_2$/acceptor UC systems achieved record normalized upconversion quantum efficiencies: (42.7 ± 0.3)%, (37.4 ± 0.2)%, (37.8 ± 0.4)% and (31.7 ± 0.2)% for DPA, CzPA, F–CzPA and CN–CzPA, respectively, according to eqn (1) (Fig. 5). To the best of our knowledge, 42.7% is the highest upconversion quantum efficiency obtained for TTA-UC using metal-based photosensitizers to date. Additionally, these values significantly exceed the efficiencies reported for Ru(II) and Cu(I) MLCT sensitizers (η_{UC} = 8–9.8% (ref. 66) and 17.8%,[48] respectively) as well as Pd(II) octaethylporphyrin (PdOEP, η_{UC} = 32% (ref. 7)) in concert with DPA. It is well established that metalloporphyrin photosensitizers undergo homomolecular triplet–triplet annihilation that serves as a competing process with respect to the desired acceptor-based TTA.[67–74] Importantly, neither homomolecular TTA nor any other self-quenching process was observed in the Zr(IV) LMCT sensitizer, whose excited state lifetime remained constant across all sensitizer concentrations investigated. For the photochemical upconversion systems using CzPA series as acceptors/annihilators, the upconversion quantum efficiencies – although they do not rival that of the benchmark DPA – are still impressive when compared to the large body of existing anthracene-based

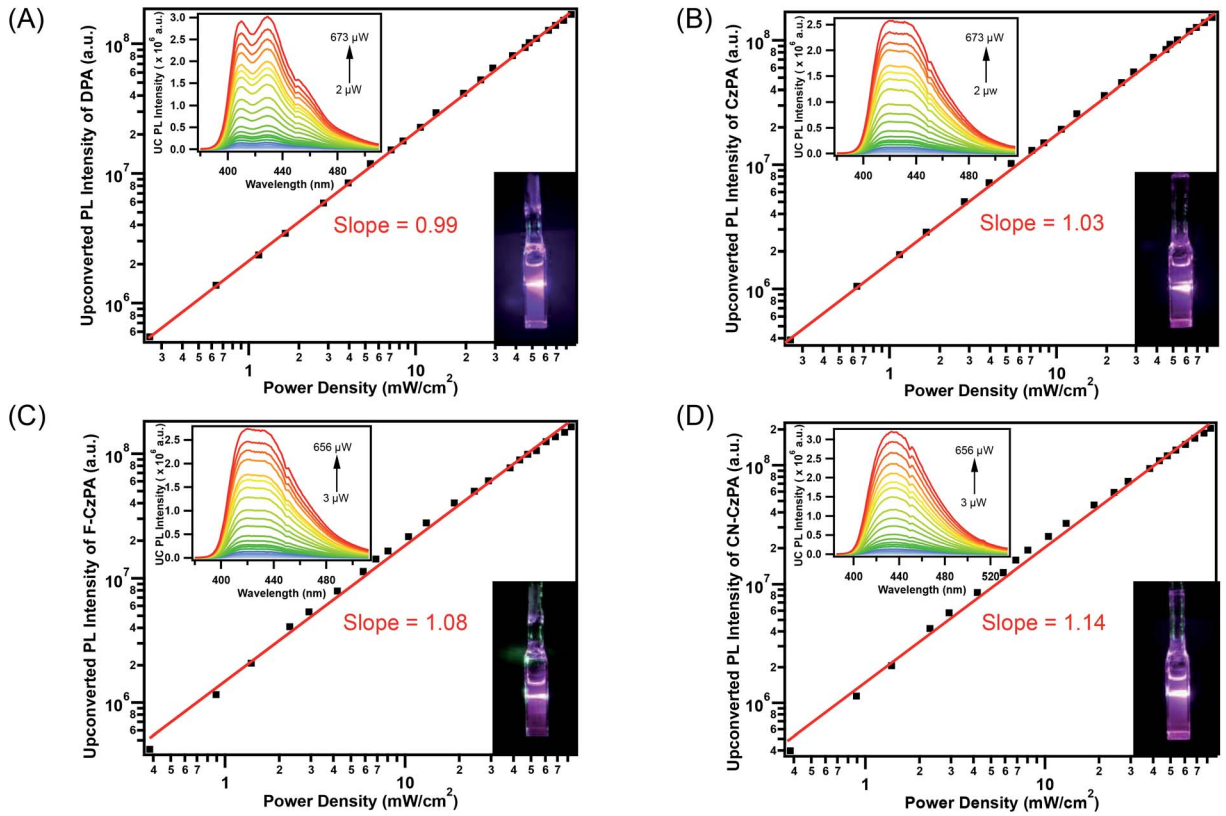

Fig. 4 Double logarithmic plot of upconverted integrated photoluminescence intensities of acceptors/annihilators, (A) DPA, (B) CzPA, (C) F–CzPA and (D) CN–CzPA, respectively, as a function of 514.5 nm excitation power densities. Solution compositions were 0.25 mM acceptors/annihilators and $Zr(^{Mes}PDP^{Ph})_2$ (OD_{514nm} – 0.2) in deaerated THF. The solid red lines represent the linear fits with slopes of 1, illustrating linear response at low power density. The upper left insets show upconverted photoluminescence spectra of the corresponding solution compositions at different excitation powers and the lower right insets show the digital photographs of upconverted photoluminescence of acceptors/annihilators under 514.5 nm excitation by using an Ar^+/Kr^+ laser.

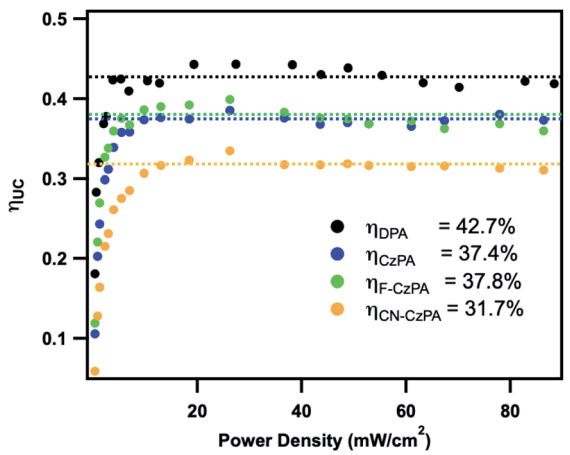

Fig. 5 Upconversion quantum efficiencies measured for 0.25 mM acceptors/annihilators sensitized by $Zr(^{Mes}PDP^{Ph})_2$ ($OD_{514\ nm} = 0.2$) in deaerated THF solutions as a function of excitation power density at 514.5 nm.

annihilators.[22,61,75–78] Interestingly, the η_{UC} values for these UC compositions are roughly proportionate to the fluorescence quantum yields (Φ_F) of the acceptor/annihilator chromophores, shown in Table 1. Considering that η_{UC} under our specific experimental conditions is the product of the quantum yields of each step in the TTA-UC mechanism, *i.e.* $\eta_{UC} = 2 \times \Phi_{ISC} \times \Phi_{TTET} \times \Phi_{TTA} \times \Phi_F$, the agreement between η_{UC} and Φ_F suggests that the η_{UC} of the current compositions appear to be limited by the fluorescence quantum yields of the acceptor/annihilator chromophores, rather than any inherent properties of the Zr(IV) sensitizer or the bimolecular energy transfer processes involved. The maximum η_{UC} of 42.7% for Zr(IV)/DPA composition is likely reflecting the maximum normalized TTA efficiency ($\eta_{TTA} = 2 \times \Phi_{TTA}$) of 40% within experimental error of the η_{UC} measurement.[70,71] The underlying mechanism of the TTA process is generally regarded as an encounter complex formation between two excited triplet acceptor/annihilator molecules. Triplet–triplet encounters yield the following spin statistics: 5/9 quintets, 3/9 triplets and 1/9 singlets.[79] Only the singlet complex can dissociate to acceptor molecules in the S_1 state producing the upconverted fluorescence. As such, 18 triplet acceptors are expected to yield 1 singlet acceptor ($\eta_{TTA} = 5.5\% \times 2 = 11\%$). However, the highly energized quintet states are not thermally accessible, eliminating 10 triplets from the statistical mix, leaving 8 triplets producing 1 singlet acceptor ($\eta_{TTA} = 12.5\% \times 2 = 25\%$). If the upper T_2 states (dissociated from the 3/9 triplet

encounter complexes) recycle into T_1 acceptors, 3 additional triplets are removed from the calculation, yielding 1 singlet acceptor being produced from 5 triplets ($\eta_{TTA} = 20\% \times 2 = 40\%$). This scenario is most consistent with the experimental data presented in Fig. 5 as well as numerous related UC systems.[7,59,80,81]

To further evaluate the upconversion performance metrics intended for non-coherent solar photon capture and conversion, we estimated the integrated solar irradiance over the lowest energy absorption band of $Zr(^{Mes}PDP^{Ph})_2$, Fig. S21.† The solar irradiance over this absorption profile is 26.7 mW cm^{-2}, which is notably larger than the 13 mW cm^{-2} required here to achieve the maximum η_{UC} in the current compositions. This illustrates that the maximum η_{UC} of the current donor–acceptor pairs can be achieved under terrestrial sunlight, highlighting the potential of these particular UC systems for real-word solar energy-based applications.

The significant advance enabling the realization of low threshold, high quantum yield photochemical upconversion clearly has its origin in the Zr(IV) photosensitizer. Besides featuring TADF which circumvents energetic losses during ISC, this chromophore possesses a large absorption cross-section in the visible ($\varepsilon_{525} = 21\,570$ M^{-1} cm^{-1}) while having an excited state lifetime of 350 μs at RT.[51] These combined properties enabled the use of low concentrations of this sensitizer, generating large K_{SV} values ($\sim 10^5$ M^{-1}) while circumventing parasitic self-quenching and aggregation as well as the reabsorption of upconverted photons. Although it is described as a ^{3}LMCT excited state, this Zr(IV) molecule possesses a somewhat complex electronic structure featuring significant triplet ligand-centred (^{3}LC) character as well. This mixed excited-state character may accommodate a larger distribution of interactions that enable TTET ultimately leading to more product-favouring collisions. This may rationalize why the K_{SV} values are quite large even though the driving force for TTET is only ~0.19 eV, which led to rate constants of 2–3 $\times$ 10^8 M^{-1} s^{-1}. Nevertheless, the combination of the newly conceived Zr(IV) photosensitizer and DPA-based acceptors/annihilators yields upconverting formulations operating with linear power dependence at low excitation power density. These donor–acceptor mixtures achieve maximum record efficiencies below the solar flux available across the Zr(IV) photosensitizer visible absorption band.

Conclusions

We describe a number of unusually efficient molecular-based photochemical upconversion compositions featuring the $Zr(^{Mes}PDP^{Ph})_2$ photosensitizer in concert with a number of DPA-based acceptors/annihilators. The initial TTET processes featured very large K_{SV} values approaching or achieving 10^5 M^{-1} with bimolecular rate constants between 2–3 $\times$ 10^8 M^{-1} s^{-1}. Conditions optimizing the TTET quantum yield generated linear UC response down to microwatt incident light power levels. Impressive record-setting η_{UC} values ranging from 31.7% to 42.7% were achieved under excitation conditions (13 mW cm^{-2}) below that of solar flux integrated across the Zr(IV) photosensitizer's absorption band (26.7 mW cm^{-2}). These observations demonstrate that maximum η_{UC} can be achieved in the current UC pairs using terrestrial sunlight, presenting enormous potential for non-coherent solar photon capture and conversion. We expect that the potential of earth-abundant early transition metal photosensitizers will inspire further exploration in future photosensitizer development for applications in solar energy conversion and light management.

Data availability

All data is in the ESI. There is no more to deposit.

Author contributions

F. N. C. and M. Y. conceived the project and designed the experiments. The experiments and data analysis including static absorption, photoluminescence, time-resolved photoluminescence spectroscopy, nanosecond transient absorption spectroscopy and photochemical upconversion were performed by M. Y. with input from F. N. C. Synthesis and structural characterization were performed by S. S. and Y. Z. Electronic structure calculations and absolute quantum yield measurements were performed by S. S. The research was supervised by F. N. C. and C. M. All authors discussed the results and progress at all stages with the manuscript being composed by all authors.

Conflicts of interest

There are no conflicts to declare.

Acknowledgements

This work was supported by the U.S. Department of Energy, Office of Science, Office of Basic Energy Sciences, under Award Number DE-SC0011979. The work performed at West Virginia University was supported by the National Science Foundation, Division of Chemistry, under Award Number CHE-1752738. We thank Dr Peter M. Thompson from the NC State Molecular Education, Technology, and Research Innovation Center (METRIC) for performing the DOSY and ROESY ^{1}H NMR experiments.

Notes and references

1 C. A. Parker and E. J. Bowen, *Proc. - R. Soc. Edinburgh, Sect. A: Math. Phys. Sci.*, 1963, **276**, 125–135.
2 C. A. Parker, in *Advances in Photochemistry*, John Wiley & Sons, Ltd, 1964, pp. 305–383.
3 C. A. Parker, C. G. Hatchard and T. A. Joyce, *Nature*, 1965, **205**, 1282–1284.
4 T. W. Schmidt and F. N. Castellano, *J. Phys. Chem. Lett.*, 2014, **5**, 4062–4072.
5 T. N. Singh-Rachford and F. N. Castellano, *Coord. Chem. Rev.*, 2010, **254**, 2560–2573.
6 Y. Zhou, F. N. Castellano, T. W. Schmidt and K. Hanson, *ACS Energy Lett.*, 2020, **5**, 2322–2326.

7 R. S. Khnayzer, J. Blumhoff, J. A. Harrington, A. Haefele, F. Deng and F. N. Castellano, *Chem. Commun.*, 2011, **48**, 209–211.
8 T. F. Schulze and T. W. Schmidt, *Energy Environ. Sci.*, 2015, **8**, 103–125.
9 L. Nienhaus, J.-P. Correa-Baena, S. Wieghold, M. Einzinger, T.-A. Lin, K. E. Shulenberger, N. D. Klein, M. Wu, V. Bulović, T. Buonassisi, M. A. Baldo and M. G. Bawendi, *ACS Energy Lett.*, 2019, **4**, 888–895.
10 D. Beery, J. P. Wheeler, A. Arcidiacono and K. Hanson, *ACS Appl. Energy Mater.*, 2020, **3**, 29–37.
11 B. D. Ravetz, A. B. Pun, E. M. Churchill, D. N. Congreve, T. Rovis and L. M. Campos, *Nature*, 2019, **565**, 343–346.
12 B. Pfund, D. M. Steffen, M. R. Schreier, M.-S. Bertrams, C. Ye, K. Börjesson, O. S. Wenger and C. Kerzig, *J. Am. Chem. Soc.*, 2020, **142**, 10468–10476.
13 M. Majek, U. Faltermeier, B. Dick, R. Pérez-Ruiz and A. Jacobi von Wangelin, *Chem. –Eur. J.*, 2015, **21**, 15496–15501.
14 R. R. Islangulov and F. N. Castellano, *Angew. Chem.*, 2006, **118**, 6103–6105.
15 Y. I. Park, K. T. Lee, Y. D. Suh and T. Hyeon, *Chem. Soc. Rev.*, 2015, **44**, 1302–1317.
16 Y. Liu, Y. Lu, X. Yang, X. Zheng, S. Wen, F. Wang, X. Vidal, J. Zhao, D. Liu, Z. Zhou, C. Ma, J. Zhou, J. A. Piper, P. Xi and D. Jin, *Nature*, 2017, **543**, 229–233.
17 A. Punjabi, X. Wu, A. Tokatli-Apollon, M. El-Rifai, H. Lee, Y. Zhang, C. Wang, Z. Liu, E. M. Chan, C. Duan and G. Han, *ACS Nano*, 2014, **8**, 10621–10630.
18 S. H. C. Askes, A. Bahreman and S. Bonnet, *Angew. Chem.*, 2014, **126**, 1047–1051.
19 N. Harada, Y. Sasaki, M. Hosoyamada, N. Kimizuka and N. Yanai, *Angew. Chem.*, 2020, **133**, 144–149.
20 D. V. Kozlov and F. N. Castellano, *Chem. Commun.*, 2004, 2860–2861.
21 S. Garakyaraghi, P. D. Crapps, C. E. McCusker and F. N. Castellano, *Inorg. Chem.*, 2016, **55**, 10628–10636.
22 K. A. E. Roz and F. N. Castellano, *Chem. Commun.*, 2017, **53**, 11705–11708.
23 C. Mongin, S. Garakyaraghi, N. Razgoniaeva, M. Zamkov and F. N. Castellano, *Science*, 2016, **351**, 369–372.
24 C. Mongin, P. Moroz, M. Zamkov and F. N. Castellano, *Nat. Chem.*, 2018, **10**, 225–230.
25 Q. Chen, Y. Liu, X. Guo, J. Peng, S. Garakyaraghi, C. M. Papa, F. N. Castellano, D. Zhao and Y. Ma, *J. Phys. Chem. A*, 2018, **122**, 6673–6682.
26 N. Awwad, A. T. Bui, E. O. Danilov and F. N. Castellano, *Chem*, 2020, **6**, 3071–3085.
27 J. R. Palmer, K. A. Wells, J. E. Yarnell, J. M. Favale and F. N. Castellano, *J. Phys. Chem. Lett.*, 2020, **11**, 5092–5099.
28 C. M. Papa, S. Garakyaraghi, D. B. Granger, J. E. Anthony and F. N. Castellano, *Chem. Sci.*, 2020, **11**, 5690–5696.
29 M. Yang, J. E. Yarnell, K. El Roz and F. N. Castellano, *ACS Appl. Energy Mater.*, 2020, **3**, 1842–1853.
30 R. R. Islangulov, D. V. Kozlov and F. N. Castellano, *Chem. Commun.*, 2005, 3776–3778.
31 K. Fujimoto, K. Kawai, S. Masuda, T. Mori, T. Aizawa, T. Inuzuka, T. Karatsu, M. Sakamoto, S. Yagai, T. Sengoku, M. Takahashi and H. Yoda, *Langmuir*, 2019, **35**, 9740–9746.
32 S. Ji, H. Guo, W. Wu, W. Wu and J. Zhao, *Angew. Chem.*, 2011, **123**, 8433–8436.
33 W. Wu, S. Ji, W. Wu, J. Shao, H. Guo, T. D. James and J. Zhao, *Chem. –Eur. J.*, 2012, **18**, 4953–4964.
34 W. Zhao and F. N. Castellano, *J. Phys. Chem. A*, 2006, **110**, 11440–11445.
35 K. A. Phillips, T. M. Stonelake, K. Chen, Y. Hou, J. Zhao, S. J. Coles, P. N. Horton, S. J. Keane, E. C. Stokes, I. A. Fallis, A. J. Hallett, S. P. O'Kell, J. M. Beames and S. J. A. Pope, *Chem. –Eur. J.*, 2018, **24**, 8577–8588.
36 S. J. Pope, C. E. Elgar, H. Y. Otaif, X. Zhang, J. Zhao, J. M. Beames, P. N. Horton and S. J. Coles, *Chem. –Eur. J.*, 2021, **27**, 3427–3439.
37 P. Duan, N. Yanai and N. Kimizuka, *Chem. Commun.*, 2014, **50**, 13111–13113.
38 X. Yi, J. Zhao, J. Sun, S. Guo and H. Zhang, *Dalton Trans.*, 2013, **42**, 2062–2074.
39 X. Yi, J. Zhao, W. Wu, D. Huang, S. Ji and J. Sun, *Dalton Trans.*, 2012, **41**, 8931–8940.
40 T. N. Singh-Rachford and F. N. Castellano, *J. Phys. Chem. Lett.*, 2010, **1**, 195–200.
41 V. Yakutkin, S. Aleshchenkov, S. Chernov, T. Miteva, G. Nelles, A. Cheprakov and S. Baluschev, *Chem. –Eur. J.*, 2008, **14**, 9846–9850.
42 T. N. Singh-Rachford and F. N. Castellano, *Inorg. Chem.*, 2009, **48**, 2541–2548.
43 O. S. Wenger, *Nat. Chem.*, 2020, **12**, 323–324.
44 J. K. McCusker, *Science*, 2019, **363**, 484–488.
45 S. Garakyaraghi, E. O. Danilov, C. E. McCusker and F. N. Castellano, *J. Phys. Chem. A*, 2015, **119**, 3181–3193.
46 S. Garakyaraghi, C. E. McCusker, S. Khan, P. Koutnik, A. T. Bui and F. N. Castellano, *Inorg. Chem.*, 2018, **57**, 2296–2307.
47 S. Garakyaraghi, P. Koutnik and F. N. Castellano, *Phys. Chem. Chem. Phys.*, 2017, **19**, 16662–16668.
48 C. E. McCusker and F. N. Castellano, *Inorg. Chem.*, 2015, **54**, 6035–6042.
49 Y. Zhang, J. L. Petersen and C. Milsmann, *J. Am. Chem. Soc.*, 2016, **138**, 13115–13118.
50 Y. Zhang, T. S. Lee, J. L. Petersen and C. Milsmann, *J. Am. Chem. Soc.*, 2018, **140**, 5934–5947.
51 Y. Zhang, T. S. Lee, J. M. Favale, D. C. Leary, J. L. Petersen, G. D. Scholes, F. N. Castellano and C. Milsmann, *Nat. Chem.*, 2020, **12**, 345–352.
52 Y. Zhang, D. C. Leary, A. M. Belldina, J. L. Petersen and C. Milsmann, *Inorg. Chem.*, 2020, **59**, 14716–14730.
53 A. Salehi, C. Dong, D.-H. Shin, L. Zhu, C. Papa, A. Thy Bui, F. N. Castellano and F. So, *Nat. Commun.*, 2019, **10**, 2305.
54 P. Ledwon, *Org. Electron.*, 2019, **75**, 105422.
55 T. Suzuki, Y. Nonaka, T. Watabe, H. Nakashima, S. Seo, S. Shitagaki and S. Yamazaki, *Jpn. J. Appl. Phys.*, 2014, **53**, 052102.
56 Y. Huang, X. Du, S. Tao, X. Yang, C.-J. Zheng, X. Zhang and C.-S. Lee, *Synth. Met.*, 2015, **203**, 49–53.

57 W. Liu, S. Ying, R. Guo, X. Qiao, P. Leng, Q. Zhang, Y. Wang, D. Ma and L. Wang, *J. Mater. Chem. C*, 2019, **7**, 1014–1021.
58 K. Suzuki, A. Kobayashi, S. Kaneko, K. Takehira, T. Yoshihara, H. Ishida, Y. Shiina, S. Oishi and S. Tobita, *Phys. Chem. Chem. Phys.*, 2009, **11**, 9850–9860.
59 F. Deng, J. Blumhoff and F. N. Castellano, *J. Phys. Chem. A*, 2013, **117**, 4412–4419.
60 R. E. Sioda, *J. Phys. Chem.*, 1968, **72**, 2322–2330.
61 V. Gray, D. Dzebo, A. Lundin, J. Alborzpour, M. Abrahamsson, B. Albinsson and K. Moth-Poulsen, *J. Mater. Chem. C*, 2015, **3**, 11111–11121.
62 A. Haefele, J. Blumhoff, R. S. Khnayzer and F. N. Castellano, *J. Phys. Chem. Lett.*, 2012, **3**, 299–303.
63 J. E. Auckett, Y. Y. Chen, T. Khoury, R. G. C. R. Clady, N. J. Ekins-Daukes, M. J. Crossley and T. W. Schmidt, *J. Phys.: Conf. Ser.*, 2009, **185**, 012002.
64 A. Monguzzi, J. Mezyk, F. Scotognella, R. Tubino and F. Meinardi, *Phys. Rev. B*, 2008, **78**, 195112.
65 A. Monguzzi, R. Tubino, S. Hoseinkhani, M. Campione and F. Meinardi, *Phys. Chem. Chem. Phys.*, 2012, **14**, 4322–4332.
66 V. Gray, D. Dzebo, M. Abrahamsson, B. Albinsson and K. Moth-Poulsen, *Phys. Chem. Chem. Phys.*, 2014, **16**, 10345–10352.
67 G. F. Stelmakh and M. P. Tsvirko, *Opt. Spectrosc.*, 1980, **49**, 278–281.
68 G. F. Stelmakh and M. P. Tsvirko, Porphyrins, *ACS Symp. Ser.*, 1986, **321**, 118–127.
69 R. P. Steer, *Res. Chem. Intermed.*, 1989, **12**, 81.
70 R. Rautela, N. K. Joshi, S. Novakovic, W. W. H. Wong, J. M. White, K. P. Ghiggino, M. F. Paige and R. P. Steer, *Phys. Chem. Chem. Phys.*, 2017, **19**, 23471–23482.
71 J. A. O'Brien, S. Rallabandi, U. Tripathy, M. F. Paige and R. P. Steer, *Chem. Phys. Lett.*, 2009, **475**, 220–222.
72 N. K. Giri, C. P. Ponce, R. P. Steer and M. F. Paige, *Chem. Phys. Lett.*, 2014, **598**, 17–22.
73 M. Maiti, B. R. Danger and R. P. Steer, *J. Phys. Chem. A*, 2009, **113**, 11318–11326.
74 D. Dzebo, K. Börjesson, V. Gray, K. Moth-Poulsen and B. Albinsson, *J. Phys. Chem. C*, 2016, **120**, 23397–23406.
75 J. M. Rowe, J. Zhu, E. M. Soderstrom, W. Xu, A. Yakovenko and A. J. Morris, *Chem. Commun.*, 2018, **54**, 7798–7801.
76 V. Gray, K. Börjesson, D. Dzebo, M. Abrahamsson, B. Albinsson and K. Moth-Poulsen, *J. Phys. Chem. C*, 2016, **120**, 19018–19026.
77 N. Nishimura, V. Gray, J. R. Allardice, Z. Zhang, A. Pershin, D. Beljonne and A. Rao, *ACS Mater. Lett.*, 2019, **1**, 660–664.
78 R. Haruki, Y. Sasaki, K. Masutani, N. Yanai and N. Kimizuka, *Chem. Commun.*, 2020, **56**, 7017–7020.
79 Y. Y. Cheng, B. Fückel, T. Khoury, R. G. C. R. Clady, M. J. Y. Tayebjee, N. J. Ekins-Daukes, M. J. Crossley and T. W. Schmidt, *J. Phys. Chem. Lett.*, 2010, **1**, 1795–1799.
80 Y. Y. Cheng, T. Khoury, R. G. C. R. Clady, M. J. Y. Tayebjee, N. J. Ekins-Daukes, M. J. Crossley and T. W. Schmidt, *Phys. Chem. Chem. Phys.*, 2009, **12**, 66–71.
81 S. Kobayashi, K. Kikuchi and H. Kokubun, *Chem. Phys. Lett.*, 1976, **42**, 494–497.
82 T. Serevičius, R. Komskis, P. Adomėnas, O. Adomėnienė, V. Jankauskas, A. Gruodis, K. Kazlauskas and S. Juršėnas, *Phys. Chem. Chem. Phys.*, 2014, **16**, 7089–7101.